Site-specific electronic structure of Pr in Pr$_{1+x}$Ba$_{2-x}$Cu$_3$O$_{7-\delta}$

U. Staub and M. Shi

Swiss Light Source, Paul Scherrer Institute, CH-5232 Villigen PSI, Switzerland

A. G. O'Conner and M. J. Kramer

Ames Laboratory, United States Department of Energy, Iowa State University, Ames, Iowa 50011

M. Knapp

Darmstadt University of Technology, Institute for Materials Science, D-64287 Darmstadt, Germany

We report on resonant x-ray powder-diffraction measurements in the vicinity of the Pr L_3 absorption edge of Pr$_{1+x}$Ba$_{2-x}$Cu$_3$O$_{7-\delta}$. The Pr site occupation has been accurately determined: $6\pm2\%$ of the Pr is on the Ba site. From an analysis of the energy dependence of selected Bragg reflections, the site-specific oxidation state of Pr has been obtained. These results are discussed in the context of models describing the suppression of superconductivity by Pr, and they indicate that Pr on the R site is responsible for T_c suppression.

I. INTRODUCTION

The suppression of superconductivity by the substitution of Y by Pr in YBa$_2$Cu$_3$O$_{7-\delta}$ (Ref. 1) has attracted great interest since the discovery of the RBa$_2$Cu$_3$O$_{7-\delta}$ series (R = Y or rare-earth),[2] which exhibits superconducting transition temperatures of $T_c \approx 91$ K. When Pr replaces Y to form the solid solution Y$_{1-y}$Pr$_y$Ba$_2$Cu$_3$O$_{7-\delta}$, T_c rapidly decreases with increasing Pr concentration and superconductivity is suppressed below 1 K for $y \approx 0.5$. Two other lanthanide ions also show exceptional behavior, namely, Tb and Ce, which only partially substitute for Y.[3] Tb has been found to be trivalent,[4] not suppressing T_c,[3] and Ce to be in its 4+ oxidation state,[5] suppressing T_c (Ref. 3) in a similar fashion as Pr. Note that we use here the concept of valence as it is determined in the x-ray absorption near-edge structure (XANES) spectra of the L_3 edges of CeO$_2$,[6] where the ground state is not tetravalent ($\nu \approx 3.5$ e), and the formal oxidation state is by definition 4+. There is no difference between the 3+ oxidation state and the trivalent state.

To explain the suppression of superconductivity by Pr in doubly layered cuprate superconductors, several scenarios have been put forward[7-12]: hole filling, magnetic pair breaking, hole localization, and effects based on (tetravalent) Pr ions occupying the Ba sites (see Fig. 1 for the crystal structure). The recent observation of superconductivity in single crystals grown by the traveling-solvent floating-zone method[13] has been used in support of models in which disorder plays an important role in T_c suppression. Support for models based on tetravalent Pr at the Ba site is provided by a recent high-energy x-ray Compton scattering experiment.[14] However, such a scenario contradicts the interpretation of transport measurements on R(Ba$_{1-z}R_z$)$_2$Cu$_3$O$_{7-\delta}$ (R = Nd and Pr).[15] These latter measurements find similar reductions in T_c for similar amounts of Nd and Pr at the Ba site, indicating that both ions are incorporated in the trivalent oxidation state. In addition, soft x-ray-absorption measurements at the oxygen K edge find a significant number of holes in an oxygen-Pr bound state.[16] Our recent x-ray-absorption results

obtained on the Pr L_3 edge of Pr$_{1+x}$Ba$_{2-x}$Cu$_3$O$_{7-\delta}$ show that the Pr valence is intermediate, localizing the same number of holes[17] as are transferred from the chains to the planes.[18,19] These x-ray results only support the hole localization models if one assumes an insignificant amount of Pr on the Ba site. Therefore, it is evident that knowledge of the Pr/Ba site occupation and the corresponding valence state of Pr on both sites would allow one to distinguish between different models. Unfortunately, standard x-ray and neutron-diffraction techniques cannot resolve this issue, due to the
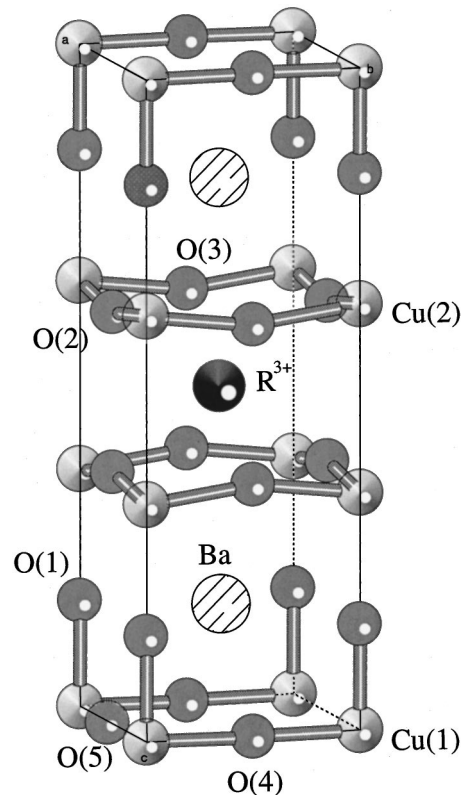
FIG. 1. Crystal structure of RBa$_2$Cu$_3$O$_{7-\delta}$.

very similar x-ray scattering factors and neutron-scattering lengths of Pr and Ba. On the other hand, spectroscopic techniques are usually not site sensitive. One may resolve the issue, however, with the combination of spectroscopy and diffraction provided by resonant x-ray scattering.

Here we present resonant x-ray powder-diffraction measurements at the Pr L_3 edge of $Pr_{1+x}Ba_{2-x}Cu_3O_{7-\delta}$. From these results, the site occupation of Pr is obtained. In addition, from the energy dependence of selected reflections, the site-specific valence of Pr is extracted, indicating that the Pr valence at the R site is significantly different from trivalent.

II. EXPERIMENTS

The $Pr_{1+x}Ba_{2-x}Cu_3O_{7-\delta}$ sample has been previously used in an x-ray-absorption study, and details on the sample preparation can be found in Ref. 17. The resonant powder-diffraction data were collected at the Hasylab B2 beamline in Hamburg, Germany, using two rectangular (5×40-cm) image plates that simultaneously covered the 2θ range 10–135 °. Halfway between the source and sample, a Pt-coated collimating mirror was inserted into the beam path to reduce the peak width, especially at high diffraction angles. A detailed description of this setup can be found in Ref. 33. The finely ground sample was glued externally onto a 1-mm capillary to reduce sample absorption of the 6-keV x rays. For energy and intensity calibrations, a 0.3-mm-diameter capillary filled with Si powder was inserted into the sample capillary, with a horizontal offset of 2 mm. The horizontal beam size was set to 14 mm, such that the beam simultaneously struck 8 mm of sample and 4 mm of Si, separated by a gap of 2 mm. This scheme allowed a direct intensity normalization of the diffraction pattern, a conversion from the pixels position on the image plate to 2θ angles and an accurate *in situ* incident photon energy calibration. The energy dependent transmission was measured by reducing the beam size to 1 $\times$0.1 mm. The entire x-ray path to the image plate was evacuated in order to reduce absorption and scattering by air. The important absorption correction in this geometry is outlined in the appendix.

III. RESULTS

Diffraction patterns were collected for 28 different energies in the vicinity of the Pr L_3 absorption edge at 5964 eV. A diffraction pattern taken at 5962 eV is shown in Fig. 2. For the refinement of the resonant powder-diffraction data, accurate values of the x-ray atomic scattering factors are required. The atomic scattering factor for an atom A can be written as

$$f_A(\mathbf{Q},E)=f_{0A}(\mathbf{Q})+f'_A(E)+if''_A(E) \qquad (1)$$

Here $f_{0A}(\mathbf{Q})$ is the scattering wave-vector dependent atomic form factor, and $f'_A(E)$ and $f''_A(E)$ are, respectively, the real and imaginary parts of the anomalous correction to the scattering factor. Due to the fact that the Ba L_1 edge (5989 eV) and the Pr L_3 edge (5964 eV) both lie in the energy range of interest, the anomalous correction factors for both ions are required for the analysis of the diffraction patterns. In principle, the imaginary part of the scattering factor that is pro-
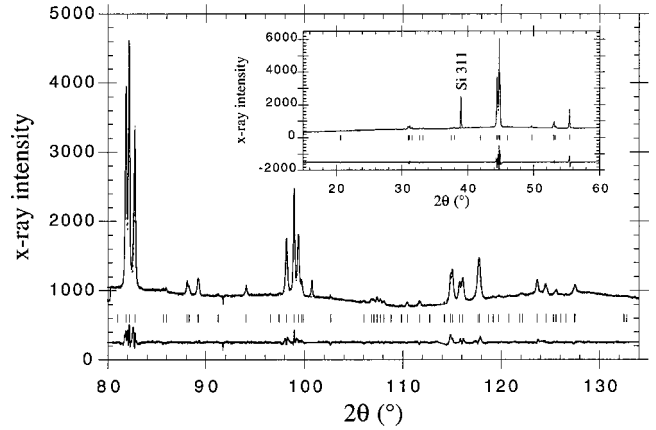
FIG. 2. X-ray-diffraction pattern, Rietveld fit, and residuals of $Pr_{1+x}Ba_{2-x}Cu_3O_{7-\delta}$, taken with an image plate at B2 of Hasylab.

portional to the mass absorption factor μ for an ion occupying a single site in the structure of interest can be obtained from XANES experiments. The electronic ground-state wave-function ψ_g of intermediate valence Pr in an oxide can be expressed as

$$\psi_g=A|4f^n\rangle + B|4f^{n+1}\underline{L}\rangle, \qquad (2)$$

with $n=1$ (and $n=0$ for Ce), where $4f^n$ and $4f^{n+1}\underline{L}$ describe the localized multielectron configurations[20,21] and $\underline{L}$ denotes a ligand hole. The valence is then directly related to the coefficients A and B, leading to different features in the XANES spectra (see Fig. 3) and thus in $f'(E)$ and $f''(E)$. In order to obtain the scattering factors for Pr from XANES, one would have to assume that the scattering factors for Pr on the R site and the Ba site are the same. In other words, the valences and the contributions of multiple scattering to the near-edge, site-selective x-ray-absorption spectra must be identical for the two sites. It is not likely that this is fully correct. However, the approximation of identical scattering
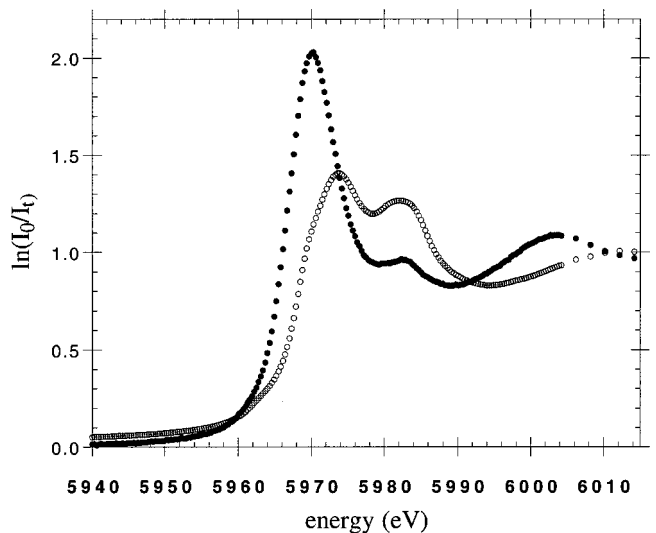
FIG. 3. X-ray-absorption near-edge structure (XANES) of the Pr L_3 edge in $Pr_{1+x}Ba_{2-x}Cu_3O_{6.97}$ (filled circles) and in formally tetravalent Pr in PrO_2 (open circles), taken at ambient temperature.
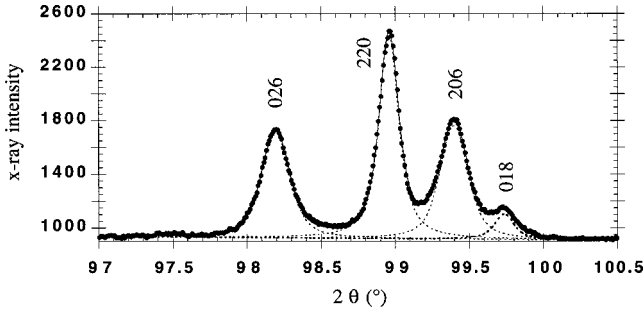
FIG. 4. The [026], [206], and [220] reflections of the x-ray-diffraction pattern showing the different linewidths of the reflections.

factors for Pr on both sites leads only to minor inaccuracies in the Rietveld refinement, since the maximum difference between the scattering factors for tri- and tetravalent Pr is much smaller than that between Ba and Pr at their resonances. As discussed below, the restriction to energies below the Pr L_3 edge (5926–5964 eV) leads to negligible differences between the scattering factors of the two valence states and therefore provides ideal conditions for the site-occupation determination. Another difficulty for the extraction of $f_A''(E)$ from the XANES data is the close proximity of the Ba L_1 and the Pr L_3 edges; they are separated by only 25 eV (see Fig. 3). Therefore, for Pr we have used the $f_{Pr}''(E)$ from the XANES in the pre-edge and white line regions. For the energy region where the Ba L_1 edge contaminates the absorption data, $f_{Pr}''(E)$ has been calculated *ab initio* with the FEFF program.[22,23] The $f_{Ba}''(E)$ values for Ba have also been calculated *ab initio*. The calculated $f_{Pr}''(E)$ is expected to be reliable above the Pr L_3 edge (in the extended x-ray-absorption fine-structure region), and the calculated $f_{Ba}''(E)$ will also be reasonably accurate. Furthermore, the Ba L_1 edge is quite weak. The real parts $f_{Pr}'(E)$ and $f_{Ba}'(E)$ are then obtained by the Kramers-Kronig transformation

$$f'(E) = \frac{2}{\pi} P \int_0^\infty \frac{d\omega' \, \omega' f''(E)}{\omega'^2 - \omega^2}, \qquad (3)$$

where P indicates the Cauchy principle part of the integral in the complex ω plane. We have used the computer code DIFFKK (Ref. 24) to obtain $f'(E)$ from $f''(E)$ for Pr and Ba in the vicinity of the two edges.

The refinement of the powder x-ray-diffraction pattern was performed with Fullprof,[25] which allows a simultaneous refinement of several patterns taken at different energies, as well as the explicit input of the scattering factors, including anomalous correction factors. All together, five patterns between 5926 and 5964 eV were used, just below the Pr L_3 edge. The first pattern to be refined was that at the lowest energy (5926.6 eV), and in order to obtain a good description of the peak shapes, an anisotropic line-broadening model was introduced. Figure 4 shows a selected region of the 5926.6 eV diffraction pattern including the [026], [206], and [220] reflections, together with a fit to Voigt functions. It is evident that the [220] reflection is narrower than the [026]

and [206] reflections. We note that in $YBa_2Cu_3O_{7-\delta}$ (not shown), this anisotropic line broadening is absent. In the fit, a single Lorentzian linewidth was assumed for all the reflections, and the Gaussian contribution was varied individually. The full width at half maximum of the [220] reflection is at 0.078(2)°, approximately half that of the [026] and the [206] reflections, which have the same width, 0.154(2)°. In general, the reflections of type $h \neq k$ are broader than those of type $h = k$, indicating microstrains along the a and b axes that are anticorrelated along the [110] direction. A similar situation has been found[26] in La_2NiO_4. Strains in connection with the tetragonal to orthorhombic phase transition in $YBa_2Cu_3O_{7-\delta}$ has been studied in detail in Refs. 27 and 28.

In order to quantitatively describe this reflection-specific line broadening, a model is adopted, which is very similar to that used[26,29] to describe the orthorhombic strain in La_2NiO_4 and the strain in the high-T_c cuprate $Pb_2Sr_2Y_{1-x}Ca_xCu_3O_{8+\delta}$. In this model, the linewidth is interpreted as a distribution of d spacings. The relevant variable for an interpretation of the diffraction pattern is the squared inverse of the lattice spacing, which is a function of the mean values of the lattice constants. The variance of $1/d_{h,k,l}^2$ can be expressed as

$$\sigma^2(1/d_{hkl}^2) = \sum_i \sum_j S_{ij} \frac{\partial(1/d_{hkl}^2)}{\partial \alpha_i} \frac{\partial(1/d_{hkl}^2)}{\partial \alpha_j}, \qquad (4)$$

where α_i corresponds to the lattice constants a, b, and c and unit-cell angles α, β, and γ, and S_{ij} is a covariance matrix. Assuming that the distributions of lattice spacing fluctuations are Gaussian, the broadening produced by the sample and the broadening from the instrumental resolution add in quadrature to produce the square of the observed peak width Γ. Therefore, Γ for the hkl reflection can be given by a modified Cagliotti expression as

$$\Gamma^2(2\theta) = (U+T)\tan^2\theta + V\tan\theta + W \qquad (5)$$

with

$$T = 8\ln 2[d_{hkl}^4 \sigma^2(1/d_{hkl}^2)], \qquad (6)$$

where U, V, and W correspond to parameters defining the instrumental resolution function. The fact that the hkl reflections with $h \neq k$ are broader than those with $h = k$ implies that S_{11}, S_{22}, and S_{21} ($= S_{12}$) are the dominant terms in the covariance matrix. This transforms Eq. (4) to

$$\sigma^2(1/d_{hkl}^2) = S_{11}\frac{4h^4}{a^6} + S_{22}\frac{4k^4}{b^6} + 2S_{12}\frac{4h^2k^2}{a^3b^3}. \qquad (7)$$

An identical Γ for the [206] and [026] reflections, and sharp reflections for $h = k$ indicate that $S_{11} = S_{22} = -S_{12}$. Because the orthorhombicity of our sample ($a = 3.8607$ Å, $b = 3.9297$ Å) is small, Eq. (7) reduces to $\sigma^2 = (4S_{11}/a^6)(h^4 + k^4 - 2h^2k^2)$. The microstrain is therefore very similar to

that found[26,30] in $La_{2-x}Sr_xNiO_4$, except for the fact that the sample is slightly orthorhombic, whereas La_2NiO_4 has a tetragonal long-range structure. This leads to a microstrain parameter $\varepsilon = \sqrt{S_{11}} = 0.8$, which is significantly smaller than the value of 4 found[26,30] in $La_{2-x}Sr_xNiO_4$.

The strain can be directly related to structural changes in $R(Ba_{1-x}R'_x)Cu_3O_{7-\delta}$, as have been found, for example, for $R = Eu$ and $R' = La$, Eu, and Pr.[31] The substitution of Ba by smaller R ions not only leads to a contraction along the c direction, but also strongly affects the a and b axes. For increasing x, a decreases and b increases until $x = 0.12$, approximately where the structural phase transition to tetragonal occurs. This is a strong indication that R substitution leads to disorder in the chains, in agreement with a soft x-ray-absorption study.[32] The fact that the length of the diagonal in the a,b plane is almost identical in the orthorhombic and tetragonal phases, in spite of significant changes in a and b, has implications for the behavior of the anisotropic strain, which must be large along [100] and [010] and small along the [110] direction. This demonstrates that a small amount of Pr on the Ba site leads to disorder of the oxygen in the chains, reducing the orthorhombicity and introducing the [100] and [010] strains.

To refine the degree of Pr occupation on the Ba site, all structural parameters were fixed to the values obtained from the refinement of the pattern taken at 5926.6 eV. The simultaneous refinement of five diffraction patterns taken at different energies allows a very accurate determination of the Pr site occupation, since it is the only parameter that is sensitive to the energy dependent changes in the scattering. We obtain a value of $x = 0.06 \pm 0.02$, which compares well with the starting composition of $x = 0.05$ of the preparation procedure. We note that in analyzing five different diffraction patterns across the Pr L_3 edge, x remains constant at 0.06. This value is in agreement with that estimated from polarized neutron diffraction,[33] however, is more directly obtained and expected to be more accurate.

In principle, resonant diffraction offers the advantage of combining spectroscopic information with the site selectivity of diffraction. Therefore, by measuring the energy dependent x-ray intensity of selected Bragg reflections in the vicinity of the edge (XANES region), information on the site-selective electronic structure of Pr can be obtained. However, due to the small concentration of only $x = 0.06$ Pr on the Ba site, and the fact that the contribution from the R site is independent of the hkl reflection, the Pr valence on the Ba site could not be extracted from the powder data with the insufficient statistics available. For the Pr at the R site, on the other hand, the situation is different. There exist reflections of type $[hk7]$ for which the contribution from Pr on the Ba site $(1/2,1/2,\pm z)$ is insignificant [proportional to $\cos(2\pi lz) = -0.08$ for $z = 0.1805$], and as we have seen, only 6% of Pr occupies this site. This makes a determination of the valence of Pr on the R site possible.

To describe the energy dependence of reflections of type $[hk7]$, we used the anomalous scattering factors from the $3+$ and $4+$ oxidation states of Pr. For the trivalent case, which exhibits a single resonance, we have used the *ab initio*
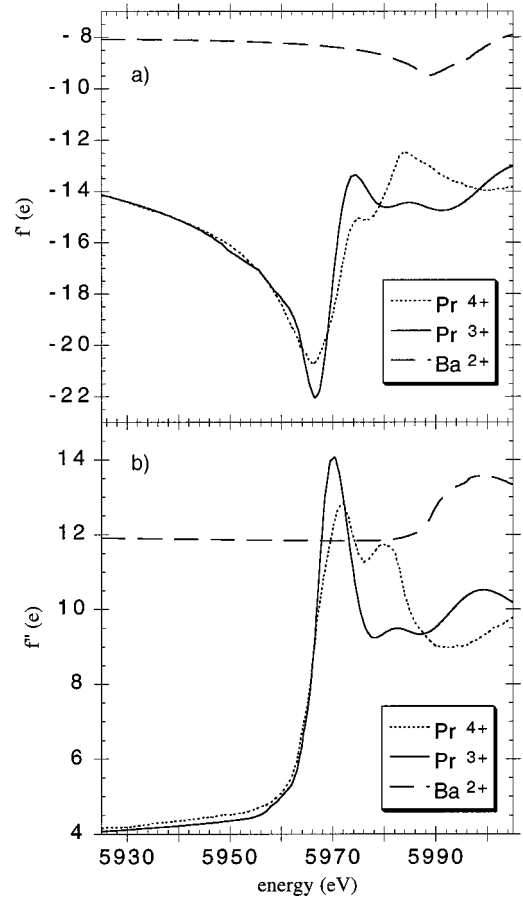
FIG. 5. Anomalous corrections to the scattering factor of Pr in the 3+ and 4+ oxidation states and of Ba, extracted from either absorption data or obtained from FEFF calculations and Kramers-Kronig transformations. Upper part (a): real parts of the anomalous correction factor. Lower part (b): imaginary parts of the anomalous correction factor.

calculated values from FEFF and the corresponding values from the Kramers-Kronig transformation for the anomalous corrections to the scattering factors. For the 4+ oxidation state of Pr, the FEFF calculation is inaccurate, and we were forced to extract the anomalous corrections from the PrO_2 XANES spectra (see Fig. 3). The resulting f'_{Pr3+}, f''_{Pr3+} and f'_{Pr4+}, f''_{Pr4+} are shown in Fig. 5. For the calculation of the [027] and [207] reflections, the atomic form factor for tri- and tetravalent Pr has been taken from Ref. 34. The energy dependence of the averaged [027] and [207] reflections is shown in Fig. 6. The site-selective Pr valence has then been obtained by fitting these data to the structure factor, using $f_{Pr} = (1-\alpha)f_{Pr3+} + \alpha f_{Pr4+}$, in analogy to a valence determination from XANES spectra. The fit of the parameter α, which is also shown in Fig. 6, results in an oxidation state for Pr at the R site of $\nu = 3 + \alpha = 3.27 \pm 0.08$, in agreement with the value for the global average oxidation state of Pr in this sample[17] of 3.23 ± 0.01 e. The average of two reflections is used in order to improve statistics.

IV. DISCUSSION

From the Pr site occupation $x = 0.06(2)$ of the Ba site, and assuming Pr^{4+} replaces Ba^{2+}, a maximum number of holes
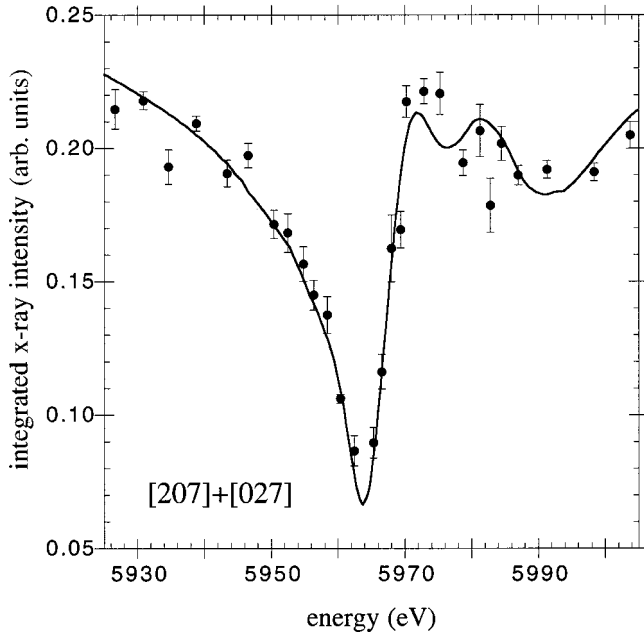
FIG. 6. Energy dependence of the integrated average intensity of the [207] and [027] reflections in the vicinity of the Pr L_3 edge. The line corresponds to a fit, determining the Pr site-selective valence at the R site.

of $n = 0.12$ per unit cell can be filled. This is at least a factor of 2 too small, when compared to the number of holes transferred from chains to planes when going from the undoped RBa$_2$Cu$_3$O$_6$ to doped RBa$_2$Cu$_3$O$_7$.[18,19] Therefore, merely from the occupancy of Pr on the Ba site, models that claim that tetravalent Pr on the Ba site suppresses (super)conductivity due to hole filling[14] can be excluded. In addition, the fact that only light rare-earth elements up to Gd (i.e., with large ionic radii) substitute for Ba (which is larger than Pr^{4+}), is a clear indication for trivalent Pr at the Ba site.

The finding that the Pr occupation on the Ba site agrees with the expected chemical stochiometry demonstrates that transport studies on carefully prepared samples, with varying Pr and Nd doping on the Ba site, can give valuable information on the effect of R substitution on T_c.[15] These measurements thus strongly indicate that both R ions have the same valence state when located at the Ba site and that they are therefore both trivalent. The model that trivalent Pr ions at the Ba sites suppress superconductivity due to pair breaking[12] is unlikely, since Eu (Ba$_{2-x}$Pr$_x$)Cu$_3$O$_{7-\delta}$ (Ref. 31) is still superconducting for $x = 0.3$, but superconductivity is already lost for $x = 0.06$ in our sample of Pr$_{1+x}$Ba$_{2-x}$Cu$_3$O$_{7\delta}$. Moreover, Pr on the Ba site has a singlet ground state due to the low site symmetry, in contrast to Nd, which has a magnetic doublet (Kramers ion) and does have a distinct smaller effect on superconductivity. As our results directly indicate that Pr localizes holes at the R site, they also strongly support models based on hole localization due to hybridization of the $4f$ orbitals with the oxygen $2p$ states.

It is very difficult to understand the questionable occurrence of superconductivity in crystals of PrBa$_2$Cu$_3$O$_{7-\delta}$,[13] where it is argued that superconductivity is restored due to

the absence of Pr on the Ba site. The size mismatch between the smaller Pr and larger Ba ions is significant and is very likely to be responsible for the anticorrelated microstrain along the a and b directions, either directly or via oxygen ions occupying the antichain sites. However, a proposal that a small localized structural distortion on the Ba site promotes the hole localization at the R site is unlikely, particularly because the $4f$ electrons form bands,[9] which are not expected to be disturbed by a few percent of disorder. Therefore, the small Pr disorder on the Ba site and the suppression of superconductivity by Pr on the R site due to hole localization can be viewed as two independent physical effects.

It is interesting to note that in the case of x-dependent T_c suppression in Y$_{1-x}$Pr$_x$Ba$_2$Cu$_3$O$_{7-\delta}$, T_c is already below 1 K for $x \approx 0.5$. Because the number of localized holes per Pr and the number of expected holes coincides for $x = 1$, the oxidation state of Pr is expected to be approximately twice as large in the vicinity of $x = 0.5$ compared to $x = 1$, which would be of the order of 3.5. Since Ce and Pr similarly suppress T_c,[3] and since Ce is known to be in the 4+ oxidation state,[5] indications are that there is an additional physical effect of T_c suppression for low Pr concentrations, such as pair breaking.

V. CONCLUSIONS

We have performed resonant x-ray powder-diffraction measurements in the vicinity of the Pr L_3 absorption edge. The Pr site occupation has been accurately determined to be $6 \pm 2\%$ of Pr on the Ba site. The observed strain along the [100] and [010] directions can be directly related to oxygen disorder in the chains, introduced by the small fraction of Pr ion in the Ba site. From an analysis of the energy dependence of selected Bragg reflections, the site-specific oxidation state of Pr at the R site has been determined to be 3.27 ± 0.08 e, corresponding to a valence of 3.12 ± 0.03 e. These results support models that are based on the hybridization of $4f$ and $2p$ orbitals, leading to hole localization at the Pr (R site) and subsequently to the suppression of superconductivity and to the unusual magnetic properties of this strongly correlated electron system.

APPENDIX

Here, we formulate the absorption correction applicable to the hollow cylinder geometry. The intensity $I[2\theta, \mu(E)]$ is corrected using a function that depends on the energy dependent absorption coefficient of the material $\mu(E)$ and the scattering angle 2θ, through the relation

$$I_{\exp}[2\theta, \mu(E)] = A[2\theta, \mu(E)]I^\circ(2\theta, E). \quad \text{(A1)}$$
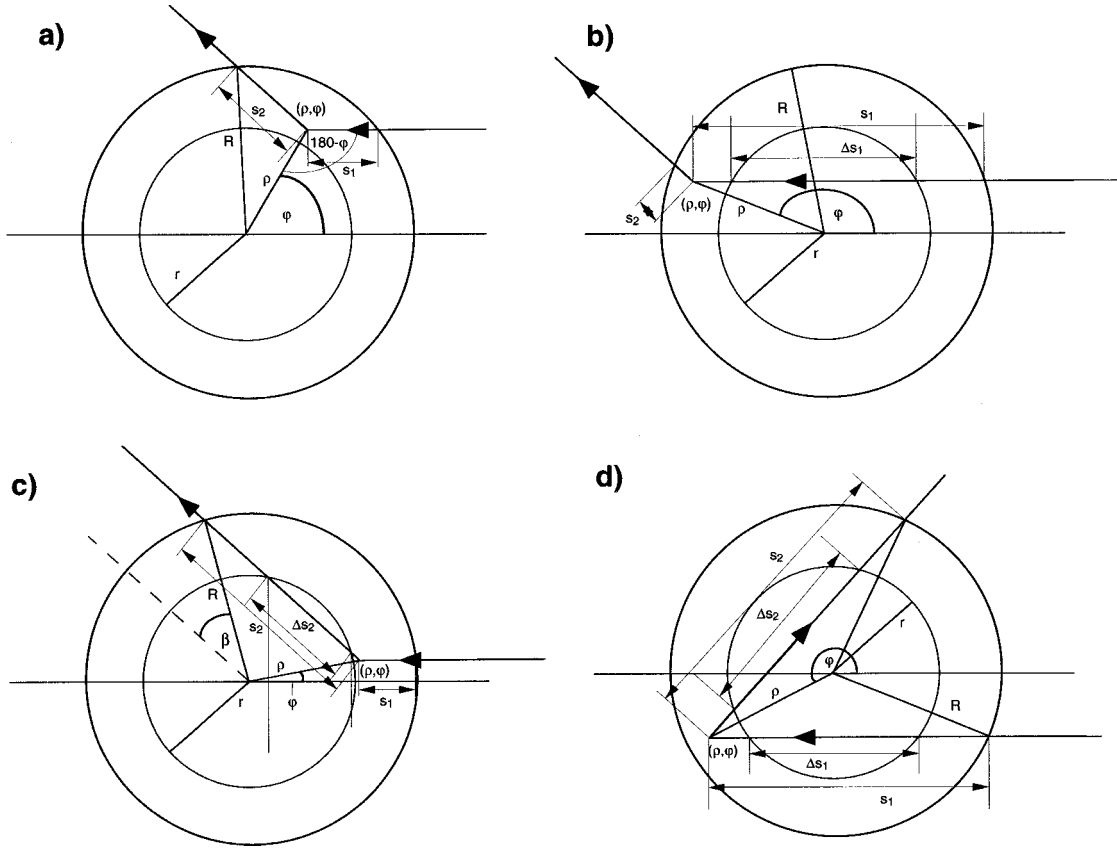
FIG. 7. (a)–(d) Sketches of the geometry of a hollow cylinder for the absorption correction, as explained in the text.

Based on the result from cylindrical geometry,[34] the function

$$A(2\theta) \propto \int_0^{2\pi} \int_r^R \exp\{-\mu[(s_1 - \Delta s_1) + (s_2 - \Delta s_2)]\}\rho \, d\rho \, d\varphi$$

(A2)

can be derived for the hollow cylinder geometry. Here $s_1(\varphi, \rho, R)$ and $\Delta s_1(\varphi, \rho, r, R)$ correspond to the path of the incoming beam into both cylinders and through the inner hollow cylinder, respectively, and $s_2(\varphi, \rho, 2\Theta, R)$ and $\Delta s_2(\varphi, \rho, 2\Theta, r, R)$ to the diffracted path going out of both cylinders and through the inner cylinder, respectively. The differences $S_1 - \Delta S_1$ and $S_2 - \Delta S_2$ are the paths of the incoming and the diffracted beams through the material, respectively. R and r represent the outer and the inner radii of the cylinders, ρ the radial location of the x-ray scattering point, and $(180 - \varphi)$ the angle between ρ and the incoming beam direction. The scattering geometries for the hollow cylinders are sketched in Fig. 7. Following Ref. 35, the parameters satisfy the following relations:

$$R \sin \alpha = \rho \sin \varphi,$$

$$R \sin \beta = \rho \sin(180° - 2\theta - \varphi),$$

$$s_1^2 = \rho^2 + R^2 - 2\rho R \cos(\varphi - \alpha),$$

$$s_2^2 = \rho^2 + R^2 + 2\rho R \cos(2\theta + \varphi + \beta).$$

(A3)

For the additional parameters Δs_1 and Δs_2 in the hollow cylinder geometry, four cases need to be considered [see Figs. 7(a)–(d)]: The x-ray path does not pass the inner cylinder ($\Delta s_1 = 0, \Delta s_2 = 0$), the incoming beam passes the inner cylinder $[\Delta s_1 = 2(r^2 - \rho^2 \sin^2 \varphi)^{1/2}, \Delta s_2 = 0]$, the scattered beam passes the inner cylinder $[\Delta s_1 = 0, \Delta s_2 = 2(r^2 - \rho^2 \sin^2 \beta)^{1/2}]$ both, and the incoming and the scattered beam pass the inner cylinder $[\Delta s_1 = 2(r^2 - \rho^2 \sin^2 \varphi)^{1/2}, \Delta s_2 = 2(r^2 - \rho^2 \sin^2 \beta)^{1/2}]$.

The function $A[2\theta, \mu(E)]$ was numerically evaluated according to Eq. (A2) and normalized to the measured transmission $A[180°, \mu(E)]$, with $r = 0.5$ mm. The diffraction patterns have then been corrected according to Eq. (A1).

[1] L. Soderholm, K. Zhang, D. G. Hinks, M. A. Beno, J. D. Jorgenson, C. U. Segre, and I. K. Schuller, Nature (London) **328**, 604 (1987).

[2] M. K. Wu, J. R. Ashburn, C. J. Torng, P. H. Hor, R. L. Meng, L. Gao, Z. J. Huang, Y. Q. Wang, and C. W. Chu, Phys. Rev. Lett. **58**, 908 (1987).

[3] C. R. Fincher, Jr. and G. B. Blanchet, Phys. Rev. Lett. **67**, 2902 (1991).

[4] U. Staub, M. R. Antonio, L. Soderholm, M. Guillaume, W. Henggeler, and A. Furrer, Phys. Rev. B **50**, 7085 (1994).

[5] U. Staub, L. Soderholm, S. Skanthakumar, and M. R. Antonio, J. Phys. IV **7**, 1077 (1997).

[6] H. Dexpert, R. C. Karnatak, J. M. Esteva, J. P. Connerade, M. Gasgnier, P. E. Caro, and L. Albert, Phys. Rev. B **36**, 1750 (1987).

[7] Y. Dalichaouch, M. S. Torikachvili, E. A. Early, B. W. Lee, C. L. Seaman, K. N. Yang, H. Zhou, and M. B. Maple, Solid State Commun. **65**, 1001 (1988).

[8] R. Fehrenbacher and T. M. Rice, Phys. Rev. Lett. **70**, 3471 (1993).

[9] A. I. Liechtenstein and I. I. Mazin, Phys. Rev. Lett. **74**, 1000 (1995).

[10] G. Y. Guo and W. M. Temmerman, Phys. Rev. B **41**, 6372 (1990).

[11] H. B. Radousky, J. Mater. Res. **7**, 1917 (1992).

[12] H. A. Blackstead and J. D. Dow, Phys. Rev. B **51**, 11 830 (1995).

[13] Z. Zou, J. Ye, K. Oka, and Y. Nishihara, Phys. Rev. Lett. **80**, 1074 (1998).

[14] A. Shukla, B. Barbiellini, A. Erb, A. Manuel, T. Buslaps, V. Honkmäki, and P. Surotti, Phys. Rev. B **59**, 12 127 (1999).

[15] M. J. Kramer, K. W. Dennis, D. Falzgraf, and R. W. McCallum, Phys. Rev. B **56**, 5512 (1997).

[16] M. Merz, N. Nuecker, E. Pellegrin, P. Schweiss, and S. Schuppler, Phys. Rev. B **55**, 9160 (1997).

[17] U. Staub, L. Soderholm, S. Skanthakumar, S. R. Wasserman, A. G. O. Conner, M. J. Kramer, B. D. Patterson, M. Shi, and M. Knapp, Phys. Rev. B **61**, 1548 (2000).

[18] M. Merz, N. Nücker, P. Schweiss, S. Schuppler, C. T. Chen, V. Chakarian, J. Freeland, Y. U. Idzerda, M. Kläser, G. Müller-Vogt, and T. Wolf, Phys. Rev. Lett. **80**, 5192 (1998).

[19] U. Staub, J. Mesot, M. Guillaume, P. Allenspach, A. Furrer, H. Mutka, Z. Bowden, and A. D. Taylor, Phys. Rev. B **50**, 4068 (1994).

[20] Z. Hu, S. Bertram, and G. Kaindl, Phys. Rev. B **49**, 39 (1994).

[21] A. Bianconi, A. Marcelli, H. Dexpert, R. Karnatak, A. Kotani, T. Jo, and J. Petiau, Phys. Rev. B **35**, 806 (1987).

[22] J. J. Rehr, J. M. d. Leon, S. I. Zabinsky, and R. C. Alberts, J. Am. Chem. Soc. **113**, 5136 (1991).

[23] S. I. Zabinsky, J. J. Rehr, A. Ankudinov, R. C. Albers, and M. J. Eller, Phys. Rev. B **52**, 2995 (1995).

[24] http://cars1.uchicago.edu/~newville/dafs/diffkk/

[25] J. Rodríguez-Carvajal, Physica B **192**, 55 (1993).

[26] J. Rodríguez-Carvajal, M. T. Fernández-Díaz, and J. L. Martínez, J. Phys.: Condens. Matter **3**, 3215 (1991).

[27] Yimei-Zhu, M. Suenaga, and A. R. Moodenbaugh, Philos. Mag. Lett. **62**, 51 (1990).

[28] K. Parlinski, V. Heine, and E. K. H. Salje, J. Phys.: Condens. Matter **5**, 497 (1993).

[29] U. Staub, L. Soderholm, S. Skanthakumar, P. Pattison, and K. Conder, Phys. Rev. B **57**, 5535 (1998).

[30] M. Medarde and J. Rodríguez-Carvajal, Z. Phys. B: Condens. Matter **102**, 307 (1997).

[31] Y. Xu, M. J. Kramer, K. W. Dennis, H. Wu, A. O'Conner, R. W. McCallum, S. K. Malik, and W. N. Yelon, Physica C **333**, 195 (2000).

[32] J. M. Chen, R. S. Liu, P. Nachimuthu, M. J. Kramer, K. W. Dennis, and R. W. McCallum, Phys. Rev. B **59**, 3855 (1999).

[33] A. J. Markvardsen, A. T. Boothroyd, B. Buck, G. J. McIntyre, and Th. Wolf, J. Magn. Magn. Mater. **177−181**, 502 (1998).

[34] E. N. Maslen, A. G. Fox, and M. A. O'Keefe, in *International Tables for Crystallography*, edited by T. Hohn (Reidel, Dordrecht, 1983).

[35] H. Ehrenberg, M. Knapp, T. Hartmann, H. Fuess, and T. Wroblewski, J. Appl. Crystallogr. **33**, 953 (2000).